HTML ABSTRACT + LINKS

APPLIED PHYSICS LETTERS VOLUME 84, NUMBER 17 26 APRIL 2004

Evolution of dislocation arrays in epitaxial $BaTiO_3$ thin films grown on (100) $SrTiO_3$

H. P. Sun, W. Tian, and X. Q. Pan[a)]
Department of Materials Science & Engineering, University of Michigan, Ann Arbor, Michigan 48109-2136

J. H. Haeni and D. G. Schlom
Department of Materials Science & Engineering, Penn State University, University Park, Pennsylvania 16802-5005

(Received 29 September 2003; accepted 1 March 2004)

Dislocation arrays and dislocation half-loops in $BaTiO_3$ thin films were characterized using transmission electron microscopy (TEM). $BaTiO_3$ films with thicknesses ranging from 2 to 20 nm were grown on (100) $SrTiO_3$ by reactive molecular beam epitaxy (MBE). The critical thickness for dislocations to occur in this system was found to lie between 2 and 4 nm. The misfit dislocations are mainly ⟨100⟩ type. The average spacing between the dislocations in the array becomes smaller when the film is thicker, which indicates gradual relaxation of mismatch strain with increasing film thickness. © *2004 American Institute of Physics.* [DOI: 10.1063/1.1728300]

Much effort has been devoted to growing epitaxial thin films on lattice-mismatched substrates for device applications. When the epilayer is thin, it is strained due to lattice mismatch. Above a critical thickness, however, dislocations are generated to reduce the mismatch strain. Dislocations, such as threading dislocation, can drastically degrade the performance of semiconductor devices. In ferroelectric oxides, the strain field surrounding dislocations can significantly perturb the ferroelectric properties of the surrounding material.[1] We are particularly interested in making epitaxial superlattices containing $BaTiO_3$ layers that are commensurately strained to the underlying $SrTiO_3$ substrate to take advantage of their enhanced ferroelectric properties.[2] It is important to know at what thickness dislocations will appear and how these dislocations move and interact with each other to reach an equilibrium configuration. In the past several decades, many theoretical models have been established to calculate the critical thickness and/or the interaction energy of dislocations.[3–10] In this letter, dislocations in epitaxial $BaTiO_3$ thin films grown on $SrTiO_3$ were studied using transmission electron microscopy (TEM).

The perovskite $BaTiO_3$ is a ferroelectric material with applications in many electronic devices including capacitors, night vision, and memory devices. Epitaxial $BaTiO_3$ thin films have been grown on $SrTiO_3$ using pulsed laser deposition (PLD),[11,12] activated reactive evaporation (ARE),[13] and metalorganic chemical vapor deposition (MOCVD).[14] Below 130 °C, unstrained $BaTiO_3$ is tetragonal ($a = 0.3992$ nm, $c = 0.4036$ nm) with a spontaneous polarization along its c axis; above 130 °C it is cubic ($a \geqslant 0.401$ nm).[15] $SrTiO_3$ is a cubic perovskite with lattice parameter $a = 0.3905$ nm at room temperature.[15] There is a 2.2% lattice mismatch for tetragonal $BaTiO_3$ on a (001) $SrTiO_3$ surface with (001)[100] $BaTiO_3$∥(001)[100] $SrTiO_3$, i.e., a c-axis-oriented epitaxial $BaTiO_3$ film. In agreement with previous work we found that the main type of misfit dislocations in such epitaxial $BaTiO_3$ thin films are interfacial edge dislocations with Burgers vector $\boldsymbol{b} = \boldsymbol{a}\langle 100\rangle$.[11] Theoretically, to completely relax the mismatch strain, the dislocation arrays should have an equilibrium configuration with a spacing of about 17.7 nm, which is calculated from b/f, in which b is the magnitude of the Burgers vector $\boldsymbol{b}$ and $f = (a_{sub} - a_{film})/a_{film}$ is the lattice mismatch between the in-plane spacing of the film, a_{film}, and that of the substrate, a_{sub}. Orthogonal arrays of dislocation lines with an average spacing of 19 nm were observed in a 200 nm thick c-axis-oriented epitaxial $BaTiO_3$ film grown on (001) $SrTiO_3$.[11] For the $BaTiO_3/SrTiO_3$ system, there is no agreement on the exact value of critical thickness. The values estimated from x-ray diffraction (XRD) are about 5 nm or less[11] and 8.7 nm.[16] Reflection high-energy electron diffraction (RHEED) revealed a value about 10 nm.[17] Theoretical calculations[11,17] following Matthews' formulas[18,19] gave 2.4–3.1 nm and 11 nm. The difference is due to the different dislocation slip systems used in the theoretical calculations. Molecular dynamics calculations[20] yielded even smaller numbers: 1.3–1.6 nm. While these calculations are for the equilibrium critical thickness, the experimental critical thickness must be at least as large as the equilibrium critical thickness and usually depends on growth conditions. It is not currently possible to precisely predict the experimental critical thickness from theoretical calculations.

In this letter, we used TEM to examine the dislocations in a series of thin epitaxial $BaTiO_3$ films grown on (001) $SrTiO_3$ with thicknesses ranging from 2 to 20 nm to see the development of dislocation arrays at the interface as a function of film thickness to relax the misfit strain. At the same time, the value of critical thickness was evaluated.

$BaTiO_3$ thin films with 2, 4, 6, 8, 12, and 20 nm thicknesses were grown on well-oriented (±0.1°) $SrTiO_3$ (001) substrates by reactive MBE. A homoepitaxial $SrTiO_3$ buffer layer about 2–4 nm thick was grown on the bare $SrTiO_3$ substrate prior to the growth of the overlying $BaTiO_3$ film. Both were grown at a substrate temperature of about 650 °C (measured using an optical pyrometer) in a background pressure of 5×10^{-7} Torr of molecular oxygen. The elemental sources, Ba and Sr contained in effusion cells and Ti from a Ti-Ball™,[21] were shuttered to deliver stoichiometric alternating monolayer doses of BaO and TiO_2 to the growth surface

[a)]Electronic mail: panx@umich.edu

 © 2004 American Institute of Physics

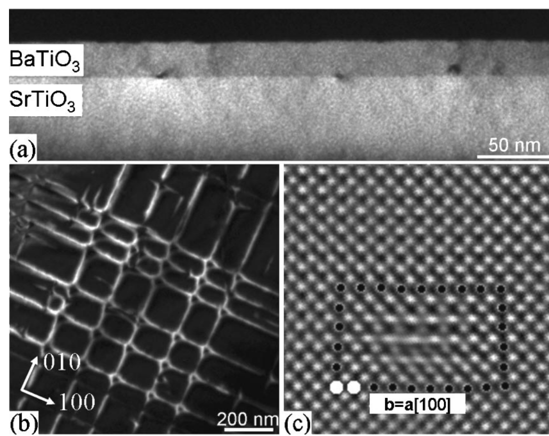

FIG. 1. (a) Cross-sectional dark-field image of a 20 nm $BaTiO_3/SrTiO_3$ film showing the dislocation cores at the interface. (b) Plane-view dark-field image of the same $BaTiO_3/SrTiO_3$ film displaying a dislocation array. (c) HRTEM image of a dislocation core at the film/substrate interface.

to build up the $BaTiO_3$ film.[22] The individual fluxes of the metallic constituents were about 1×10^{14} atoms/cm$^2\cdot$s. Cross-section and plane-view TEM samples were prepared by mechanical polishing followed by argon ion milling (PIPS, Gatan, Inc.). The plane-view samples were ion milled from the $SrTiO_3$ side. JEOL4000 and JEOL2010F TEMs were used in this work.

Figure 1(a) is a cross-sectional dark-field image of a 20 nm $BaTiO_3$ film grown on (001) $SrTiO_3$ substrate. This image was taken under $\boldsymbol{g}=(200)$ two-beam conditions. The dislocation cores at the $BaTiO_3/SrTiO_3$ interface are seen at the interface. Figure 1(b) is a dark-field image of a dislocation array in the same sample under a $\boldsymbol{g}=(110)$ two-beam condition. The area imaged includes both $BaTiO_3$ and $SrTiO_3$, which was confirmed by chemical analysis using x-ray energy dispersion spectroscopy (EDS) attached to the TEM. The orthogonal dislocation network is composed of two perpendicular edge dislocation lines with Burgers vectors $\boldsymbol{b}=\boldsymbol{a}[100]$ and $\boldsymbol{b}=\boldsymbol{a}[010]$, respectively. The Burgers vectors were determined by using the $\boldsymbol{g}\cdot\boldsymbol{b}=0$ extinction criterion under several different two-beam conditions. The atomic structure of the dislocation core at the interface was revealed in a high-resolution image, as shown in Fig. 1(c), in which the Burgers vector is determined to be $\boldsymbol{b}=\boldsymbol{a}[100]$ by drawing a Burgers circuit around the dislocation core. The bright short lines in Fig. 1(b) are dislocation half-loops which have the Burgers vector of $\boldsymbol{a}[100]$.

Figures 2(a)–2(f) are plane-view TEM images of different $BaTiO_3/SrTiO_3$ films showing the configuration and the morphology of the dislocations as a function of film thickness. The average spacing of these dislocation lines decreases with increasing film thickness, which is qualitatively in agreement with previous theoretical calculations.[7] Between the long straight lines are many isolated short defects that are dislocation half-loops which are confirmed by diffraction contrast images from both plane-view and cross-section samples and HRTEM images of cross-section sample. It should be noted that the long, straight dislocation lines in the 2 and 4 nm films are dislocations originating from the terminating points of bulk dislocations in $SrTiO_3$ substrate. The density of such bulk dislocations is consistent with the 10^6 dislocations/cm^2 typical of $SrTiO_3$ single crys-

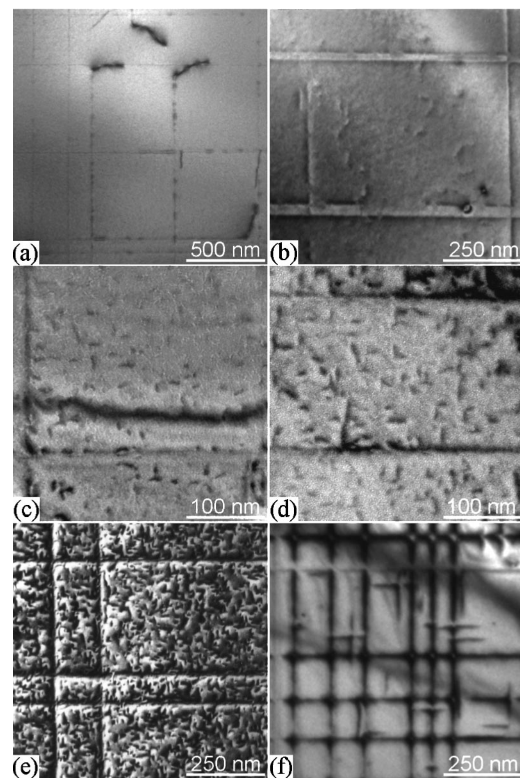

FIG. 2. Plane-view dark-field images of $BaTiO_3/SrTiO_3$ films with different thicknesses (a) 2 nm; (b) 4 nm; (c) 6 nm; (d) 8 nm; (e) 12 nm; and (f) 20 nm. It is seen that the density of straight misfit dislocations and half-loops varies with the increase of film thickness.

tals grown by the flame-fusion (Verneuil) method,[23] as is the case of the substrates used in this study. The 2 nm thick $BaTiO_3$ film was completely free of dislocation half-loops [Fig. 2(a)]. The morphology of the 4 nm film is similar to the 2 nm film except that the nuclei of dislocation half-loops become visible in the film, as shown in Fig. 2(b). So, the critical thickness for the formation of misfit dislocations in the $BaTiO_3$ thin film grown on (001) $SrTiO_3$ is between 2 and 4 nm and close to 4 nm. The measured average densities of dislocation half-loops for the films with different thicknesses are given in Table I.

Dislocation half-loops are comprised of two threading dislocations and a segment of an edge dislocation. The threading dislocation is inclined or perpendicular to the interface, while the edge part is parallel to the interface. A half-loop is formed when atoms are removed from the (100) or (010) plane of the $BaTiO_3$. The dislocation half-loop generally nucleates at the film surface and then expands toward the interface.[18] Two or more half-loops may meet and combine to form a long straight edge dislocation line at the interface. This helps to relax the misfit strain. The threading dislocation portion of the half-loop does not contribute much to strain relaxation. Through such dislocation reactions, the threading dislocations are annihilated from the film, improv-

TABLE I. Density of dislocation half-loops in $BaTiO_3$ thin films with different thickness.

Film thickness (nm)	2	4	6	8	12	20
Dislocation half-loop density (μm^{-2})	0	40	650	680	720	10

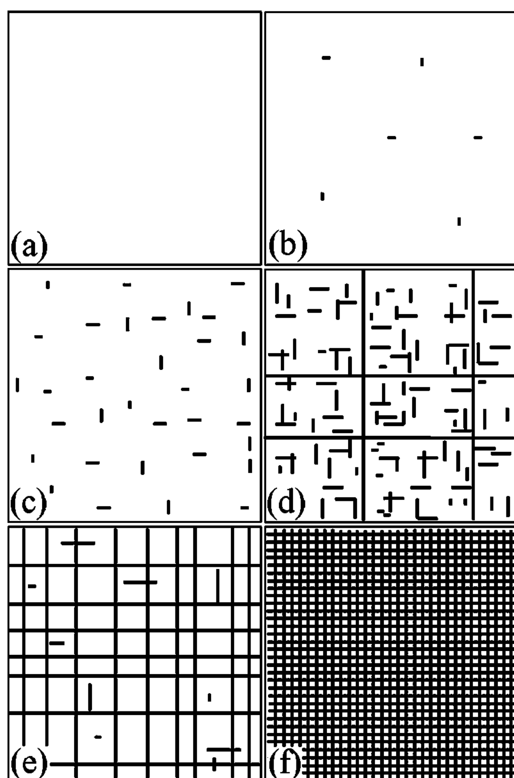

FIG. 3. Illustration of the evolution of dislocation arrays with increasing film thickness. (a) strained film free of dislocation with thickness less than the critical thickness; (b) dislocation half-loops start to nucleate when the thickness is above the critical thickness; (c) density of half-loops increases with increasing film thickness; (d) combination of dislocation half-loops into dislocation lines at the interface; (e) formation of dislocation array at the interface with decreasing number of half-loops in the film; and (f) complete relaxation of misfit strain by formation a high density and regular dislocation array at the interface.

ing the film quality. We note that inclined threading dislocations with Burgers vectors of type $\boldsymbol{a}\langle 110\rangle$ were identified to relax the misfit strain in a 200 nm thick film.[11] Its contribution to strain relaxation is insignificant in very thin films such as those studied in the present work because the small film thickness limits the length of the inclined threading dislocation along the film normal. Thus, the combination of dislocation half-loops to form a dislocation line at the interface plays a dominant role in strain relaxation for ultrathin films.

Figure 3 schematically illustrates the evolution of dislocation arrays driven by misfit strain as a function of film thickness. When the film thickness is less than the critical thickness, the film is highly strained by elastic deformation and the film is free of dislocations, as shown in Fig. 3(a). Only surface defects from the substrate can generate dislocation lines at the interface (not shown in the figure). When the film exceeds the critical thickness, dislocation half-loop begin to appear in the film, as shown in Fig. 3(b), and the length of the half-loops is short. As the film thickness increases, the population of dislocation half-loops will increase, as shown in Fig. 3(c). At a certain point, the density of dislocation half-loops is high enough and these half-loops may grow and combine together to form a long straight dislocation line at the interface that will become part of the dislocation array [Fig. 3(d)]. Gradually the average spacing of the array becomes smaller as more and more lines are formed. At the same time, new half-loops continue to nucleate at the film surface and grow. But, at some point, the rate of combination exceeds that of nucleation. So, the total number of half-loops in the film will decrease with increasing film thickness; see Fig. 3(e). The nucleation, growth, and combination of half-loops are a continuous process during the growth of the film. The dominant driving force is strain energy, which is proportional to the film thickness. By forming the dislocation arrays, the misfit strain is gradually relaxed. When the film is thick enough, at least larger than 200 nm,[11] a very regular dislocation network with 17.7 nm spacing will form to completely relax the strain, as shown in Fig. 3(f).

In conclusion, the critical thickness of c-axis-oriented epitaxial $BaTiO_3$ thin films grown on (100) $SrTiO_3$ by MBE at 650 °C is between 2 and 4 nm, and closer to 4 nm. The formation of the dislocation array is via the generation of and reaction between dislocation half-loops. The percentage of misfit strain relaxation through the formation of a dislocation array is a function of film thickness, which indicates gradual relaxation of mismatch strain with increasing film thickness.

The authors gratefully acknowledge the financial support of the National Science Foundation (NSF) through Grants DMR-0103354 and DMR-0308012. The TEM work was performed by using a JEOL 2010F TEM with NSF Award Number DMR-9871177 in the Electron Microbeam Analysis Laboratory (EMAL) at the University of Michigan. One of the authors (H.P.S.) would like to thank Dr. Corinna Wauchope and Dr. John Mansfield for assistance during use of the TEM.

[1] C. L. Canedy, H. Li, S. P. Alpay, L. Salamanca-Riba, A. L. Roytburd, and R. Ramesh, Appl. Phys. Lett. **77**, 1695 (2000).
[2] J. B. Neaton and K. M. Rabe, Appl. Phys. Lett. **82**, 1586 (2003).
[3] F. C. Frank and J. H. Van der Merwe, Proc. R. Soc. London, Ser. A **198**, 261 (1949).
[4] J. W. Matthews and A. E. Blakeslee, J. Cryst. Growth **27**, 118 (1974).
[5] R. People and J. C. Bean, Appl. Phys. Lett. **47**, 322 (1985).
[6] T. Y. Zhang, S. Lee, L. J. Guido, and C.-H. Hsueh, J. Appl. Phys. **85**, 7579 (1999).
[7] A. Rocket and C. J. Kiely, Phys. Rev. B **44**, 1154 (1991).
[8] S. D. Wang, J. Appl. Phys. **88**, 7089 (2000).
[9] M. Yu. Gutkin, K. N. Mikaelyan, and I. A. Ovid'ko, Phys. Solid State **40**, 1864 (1998).
[10] L. B. Hovakimian and S.-I. Tanaka, J. Cryst. Growth **198/199**, 900 (1999).
[11] T. Suzuki, Y. Nishi, and M. Fujimoto, Philos. Mag. A **79**, 2461 (1999).
[12] W. J. Lin, T. Y. Tseng, H. B. Lu, S. L. Tu, S. J. Yang, and I. N. Lin, J. Appl. Phys. **77**, 6466 (1995).
[13] K. Iijima, T. Terashima, K. Yamamoto, K. Hirata, and Y. Bando, Appl. Phys. Lett. **56**, 527 (1990).
[14] J. Zhang, D. Cui, H. Lu, Z. Chen, Y. Zhou, L. Li, G. Yang, S. Martin, and P. Hess, Jpn. J. Appl. Phys., Part 1 **36**, 276 (1997).
[15] *Landolt-Börnstein: Numerical Data and Functional Relationships in Science and Technology*, Vol. 16, edited by K.-H. Hellwege and A. M. Hellwege (Springer, Heidelberg, 1981), Part a, pp. 59, 67, 330.
[16] H. Terauchi, Y. Watanabe, H. Kasatani, K. Kamigaki, Y. Yano, T. Terashima, and Y. Bando, J. Phys. Soc. Jpn. **61**, 2194 (1992).
[17] G. H. Lee, B. C. Shin, and I. S. Kim, Mater. Lett. **50**, 134 (2001).
[18] J. W. Matthews, J. Vac. Sci. Technol. **12**, 126 (1975).
[19] J. W. Matthews and A. E. Blakeslee, J. Cryst. Growth **177**, 2469 (1997).
[20] W. Wunderlich, M. Fujimoto, and H. Ohsato, Thin Solid Films **375**, 9 (2000).
[21] C. D. Theis and D. G. Schlom, J. Vac. Sci. Technol. A **14**, 2677 (1996).
[22] J. H. Haeni, C. D. Theis, and D. G. Schlom, J. Electroceram. **4**, 385 (2000).
[23] A. E. Paladino, L. G. Rubin, and J. S. Waugh, J. Phys. Chem. Solids **26**, 391 (1965).